

Critical behavior of quasi-two-dimensional ferromagnet $Cr_{1.04}Te_2$

Wei Niu(钮伟), Qin-Xin Song(宋沁心), Shi-Qi Chang(常世琦), Min Wang(王敏), Kui Yuan(袁奎), Jia-Cheng Gao(高嘉程), Shuo Wang(王硕), Zhen-Dong Wang(王振东), Kai-Fei Liu(刘凯斐), Ping Liu(刘萍), Yong-Bing Xu(徐永兵), Xiao-Qian Zhang(张晓倩), and Yong Pu(普勇)

Citation: Chin. Phys. B, 2024, 33 (**7**): 077506. DOI: 10.1088/1674-1056/ad4cd8
Journal homepage: http://cpb.iphy.ac.cn; http://iopscience.iop.org/cpb

What follows is a list of articles you may be interested in

Critical behavior in the itinerant ferromagnet $SmMn_2Ge_2$

Qingyi Hou(侯清漪), Meng Song(宋猛), Xitong Xu(许锡童), Yihao Wang(王宜豪), Chao Dong(董超), Yinfa Feng(冯寅发), Miao He(何苗), Yonglai Liu(刘永来), Liang Cao(曹亮), Junfeng Wang(王俊峰), Zhe Qu(屈哲), and Yimin Xiong(熊奕敏)

Chin. Phys. B, 2023, 32 (**8**): 087501. DOI: 10.1088/1674-1056/accb49

Critical behavior and effect of Sr substitution in double perovskite Ca_2CrSbO_6

Yuan-Yuan Jiao(焦媛媛), Jian-Ping Sun(孙建平), and Qi Cui(崔琦)

Chin. Phys. B, 2021, 30 (**3**): 037501. DOI: 10.1088/1674-1056/abc67b

Critical behavior in the layered organic-inorganic hybrid $(CH_3NH_3)_2CuCl_4$

Tina Raoufi, Yinina Ma(马怡妮娜), Young Sun(孙阳)

Chin. Phys. B, 2020, 29 (**6**): 067503. DOI: 10.1088/1674-1056/ab892c

Magnetocaloric effect and critical behavior of the Mn-rich itinerant material Mn_3GaC with enhanced ferromagnetic interaction

Pengfei Liu(刘鹏飞), Jie Peng(彭杰), Mianqi Xue(薛面起), Bosen Wang(王铂森)

Chin. Phys. B, 2020, 29 (**4**): 047503. DOI: 10.1088/1674-1056/ab7da1

Critical behavior and magnetocaloric effect in magnetic Weyl semimetal candidate $Co_{2-x}ZrSn$

Tianlin Yu(于天麟), Xiaoyun Yu(余骁昀), En Yang(杨恩), Chang Sun(孙畅), Xiao Zhang(张晓), Ming Lei(雷鸣)

Chin. Phys. B, 2019, 28 (**6**): 067501. DOI: 10.1088/1674-1056/28/6/067501

RAPID COMMUNICATION

Critical behavior of quasi-two-dimensional ferromagnet $Cr_{1.04}Te_2$

Wei Niu(钮伟)[1,†], Qin-Xin Song(宋沁心)[1], Shi-Qi Chang(常世琦)[1], Min Wang(王敏)[1], Kui Yuan(袁奎)[1], Jia-Cheng Gao(高嘉程)[1], Shuo Wang(王硕)[1], Zhen-Dong Wang(王振东)[1], Kai-Fei Liu(刘凯斐)[1], Ping Liu(刘萍)[1], Yong-Bing Xu(徐永兵)[1,2], Xiao-Qian Zhang(张晓倩)[3,‡], and Yong Pu(普勇)[1,§]

[1] *Jiangsu Provincial Engineering Research Center of Low Dimensional Physics and New Energy & School of Science, Nanjing University of Posts and Telecommunications, Nanjing* 210023, *China*

[2] *School of Electronic Science and Engineering, Nanjing University, Nanjing* 210023, *China*

[3] *Key Laboratory of Quantum Materials and Devices of Ministry of Education, School of Physics, Southeast University, Nanjing* 211189, *China*

(Received 17 March 2024; revised manuscript received 15 May 2024; accepted manuscript online 17 May 2024)

The self-intercalation of Cr into pristine two-dimensional (2D) van der Waals ferromagnetic $CrTe_2$, which forms chromium tellurides (Cr_xTe_2), has garnered interest due to their remarkable magnetic characteristics and the wide variety of chemical compositions available. Here, comprehensive basic characterization and magnetic studies are conducted on quasi-2D ferromagnetic $Cr_{1.04}Te_2$ crystals. Measurements of the isothermal magnetization curves are conducted around the critical temperature to systematically investigate the critical behavior. Specifically, the critical exponents $\beta = 0.2399$, $\gamma = 0.859$, and $\delta = 4.3498$, as well as the Curie temperature $T_C = 249.56$ K, are determined using various methods, including the modified Arrott plots, the Kouvel–Fisher method, the Widom scaling method, and the critical isotherm analysis. These results indicate that the tricritical mean-field model accurately represents the critical behavior of $Cr_{1.04}Te_2$. A magnetic phase diagram with tricritical phenomenon is thus constructed. Further investigations confirm that the critical exponents obtained conform to the scalar equation near T_C, indicating their self-consistency and reliability. Our work sheds light on the magnetic properties of quasi-2D $Cr_{1.04}Te_2$, broadening the scope of the van der Waals crystals for developments of future spintronic devices operable at room temperature.

Keywords: critical behavior, van der Waals magnets, self-intercalation, magnetic measurement

PACS: 75.30.–m, 75.40.Cx, 75.30.Kz, 77.80.B– **DOI:** 10.1088/1674-1056/ad4cd8

1. Introduction

Two-dimensional (2D) magnetic van der Waals (vdW) materials hold significant promise for spintronic device applications.[1–6] Ongoing research on 2D vdW ferromagnets has led to the discovery of numerous materials,[7–11] such as Fe_3GaTe_2[12,13] and $CrTe_2$,[14] which have the Curie temperature (T_C) above the room temperature. In recent years, the binary chromium chalcogenides have drawn significant interest due to their outstanding magnetic, transport, and optical properties.[14–17] Notably, not all divalent chromium sulfides exhibit ferromagnetism; tellurides are typically ferromagnetic, whereas sulfides and selenides often manifest as antiferromagnetic metals or semiconductors.[18,19] These tellurides, with their T_C around room temperature, stand out as potential high-performance candidates for spintronic devices.[20]

Among them, 2D vdW $CrTe_2$, known for its room-temperature intrinsic ferromagnetism and pronounced perpendicular magnetic anisotropy, is essential for various spintronic devices.[14,21–24] With decreasing thickness, $CrTe_2$ exhibits layer-dependent magnetic anisotropy transition and anomalous thickness dependence of T_C.[25,26] Recently, giant topological Hall effect (THE)[27,28] and spin–orbit torque devices[29,30] have been realized in $CrTe_2$-based all vdW heterostructures. More intriguingly, the vdW gaps in $CrTe_2$ readily accommodate Cr atoms in various concentrations through the self-intercalation process,[31] resulting in a rich family of binary chromium tellurides, Cr_xTe_2, such as CrTe,[32] $Cr_{0.87}Te$,[33] Cr_5Te_6,[15] Cr_4Te_5,[34] Cr_3Te_4,[35] Cr_2Te_3,[36] Cr_5Te_8,[16] $Cr_{0.62}Te$,[37] $Cr_{1.2}Te_2$,[38,39] $Cr_{4.14}Te_8$,[40] and $CrTe_3$.[41] The quantity of Cr atoms intercalated significantly affects the crystal structure and T_C, offering an additional way to modify their properties. For example, colossal anomalous Hall effect and emergent antiferromagnetic orderings are demonstrated in Cr_5Te_8.[16,42] Room-temperature skyrmions have been observed as a result of the self-intercalation.[31,43] Depending on the Cr concentration, T_C typically ranges from 180 K to 340 K across Cr_xTe_2 variations, meanwhile, the easy axis orientation varies between the in-plane and the out-of-plane.[16,20,34,36,40,44]

Exploring critical behaviors near the phase transition from paramagnetic to ferromagnetic states offers significant insights into magnetic interactions. These behaviors, described by statistical exponents β, γ, and δ, shed light on

†Corresponding author. E-mail: weiniu@njupt.edu.cn
‡Corresponding author. E-mail: xiaoqianqian_zhang@163.com
§Corresponding author. E-mail: puyong@njupt.edu.cn

© 2024 Chinese Physical Society and IOP Publishing Ltd

the critical temperature, spin dimensionality, and interaction range.[45–49] Earlier investigations have identified variations in the critical behavior of Cr_xTe_2 components: trigonal-Cr_5Te_8 ($x = 1.25$) exhibits the 3D Ising critical behavior,[50] while the spin interactions in Cr_5Te_6 ($x = 1.67$) span the continuum from the mean-field model to the 3D Heisenberg one.[51] Additionally, long-range magnetic interaction of 3D Heisenberg model is demonstrated for Cr_4Te_5 ($x = 1.6$) bulk, despite a similar Cr concentration to Cr_5Te_6.[34] However, when forming the Cr_4Te_5 thin films, the critical behavior stands out as distinct from any typical universality class due to the magnetic disorders.[52] The variability and puzzling discrepancies of these reports call for further study of the magnetic properties of the Cr-intercalated $CrTe_2$. Moreover, recent findings indicate a notable decrease in critical temperature from 320 K to 203 K when the $CrTe_2$ is intercalated to be $Cr_{4.14}Te_8$ with such low intercalated Cr concentration (3.5%).[40] Yet, detailed understanding of Cr_xTe_2 variants with minimal Cr intercalation, especially their critical behavior, remains scarce.

Herein, this study thoroughly explores the fundamental magnetic properties of the quasi-2D $Cr_{1.04}Te_2$ single crystal. The T_C of $Cr_{1.04}Te_2$, reduced to 250 K due to Cr intercalation, contrasts with that of 2D vdW $CrTe_2$. The critical phenomenon before and after the phase transition has been explored through isothermal magnetization curve measurements. Employing various techniques, including the modified Arrott plots (MAP), the Kouvel–Fisher (KF) method, the Widom scaling method, and the critical isotherm analysis, we find that the critical exponents of $Cr_{1.04}Te_2$ correspond to the theoretical prediction of the tricritical mean-field model, which suggests long-range magnetic interactions. A corresponding magnetic phase diagram is also constructed. Our findings enhance the understanding of the magnetic properties of quasi-2D Cr_xTe_2 materials, particularly those with low Cr intercalation levels.

2. Results and discussion

The lattice structure of $Cr_{1.04}Te_2$ is schematically displayed in Fig. 1(a). An octahedral framework formed by Cr and Te atoms features a few Cr ions inserted between the layers of $CrTe_2$, which is similar to the one of $Cr_{4.14}Te_8$.[40] Figure 1(b) illustrates the Raman spectrum of the $Cr_{1.04}Te_2$ flake, displaying two main peaks at around 117 cm^{-1} (E_{2g}) and 137 cm^{-1} (A_{1g}). This is similar to that of the parent material of $CrTe_2$.[25,28] The inset is an optical picture of a $Cr_{1.04}Te_2$ crystal, which shows a metallic luster. As shown in Fig. 1(c), the energy-dispersive x-ray (EDX) spectrum validates the composition of $Cr_{1.04}Te_2$, i.e., Cr:Te = 23.6:45.4. The samples were further analyzed by scanning electron microscope (SEM) with EDX mapping. Figure 1(d) shows the SEM image of $CrTe_2$ crystals, and Figs. 1(e) and 1(f) show the distributions of Cr and Te elements, respectively. It is clear that the elemental distribution is quite uniform.

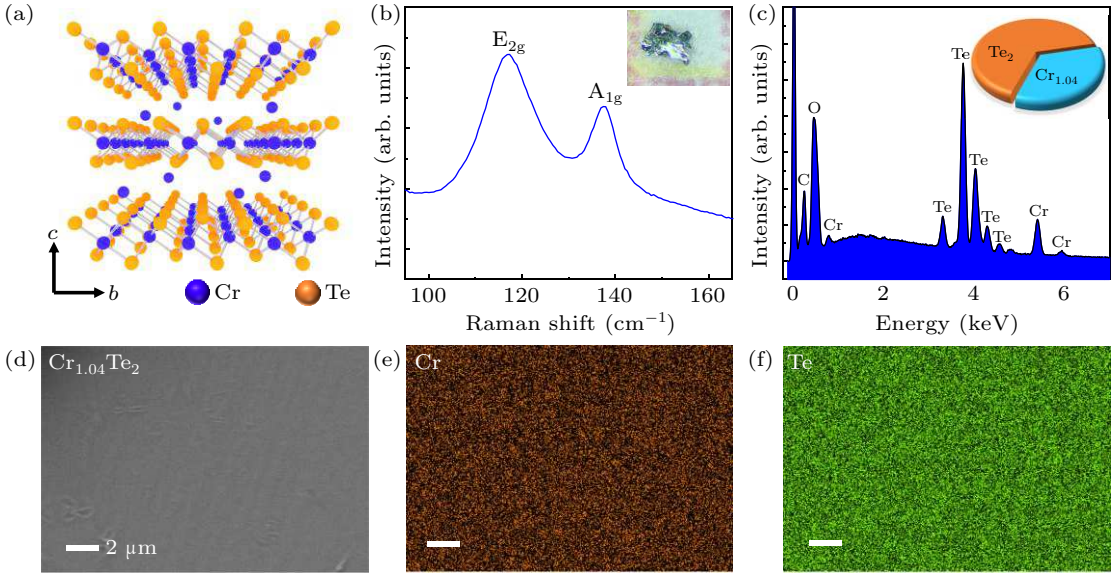


Fig. 1. (a) Lattice structure of the $Cr_{1.04}Te_2$ crystal. Some Cr atoms are inserted among vdW gaps. (b) Raman spectrum of $Cr_{1.04}Te_2$. The optical image of the $Cr_{1.04}Te_2$ is shown in the inset. (c) EDX spectrum of the $Cr_{1.04}Te_2$. The stoichiometric ratio of Cr:Te is 23.6:45.4. (d)–(f) The corresponding SEM and EDX mappings of the $Cr_{1.04}Te_2$.

We investigated the magnetic properties of $Cr_{1.04}Te_2$ by measuring the temperature (T) dependence of magnetization (M) in both in-plane and out-of-plane directions under a 500 Oe magnetic field, as shown in Fig. 2(a). This reveals an obvious phase transition from ferromagnetic to paramagnetic states as the temperature increases. The T_C, determined by the minimum of the first derivative of the M–T curve, is 252.9 K. It should be noted that the presence of

intercalated Cr atoms within the vdW gaps lowers the T_C of $Cr_{1.04}Te_2$ compared to that of $CrTe_2$, a phenomenon also observed in $Cr_{4.14}Te_8$.[40] Figure 2(b) presents the isothermal magnetization (M–H curves) under magnetic fields up to 5 T for both in-plane and out-of-plane configurations at 10 K. The in-plane magnetization approaches saturation near 20 kOe, whereas the out-of-plane magnetization continues to increase up to 50 kOe, suggesting that the easy-axis of $Cr_{1.04}Te_2$ is in-plane. This characteristic aligns with those of bulk $CrTe_2$[22] and $Cr_{4.14}Te_8$,[40] yet contrasts with other Cr_xTe_2 compounds, such as Cr_5Te_8[16] and Cr_3Te_4,[44] which share an out-of-plane easy axis.

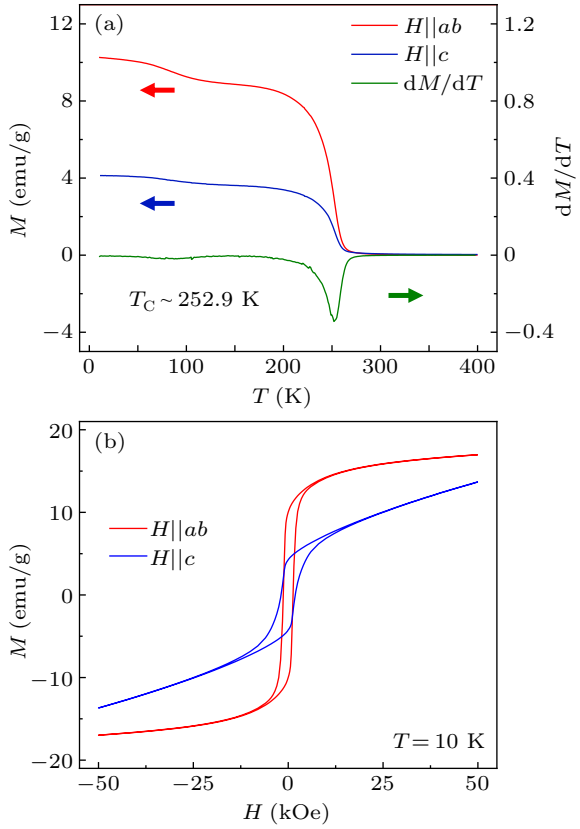


Fig. 2. (a) Temperature dependence of in-plane and out-of-plane magnetization of $Cr_{1.04}Te_2$, respectively. The applied field is 500 Oe. The green curve is the first derivative of the magnetization as a function of the temperature. (b) Isothermal magnetization, M–H, loops of $Cr_{1.04}Te_2$ measured at a typical temperature of 10 K for both $H\|ab$ and $H\|c$.

To delve into the nature of the ferromagnetic phase transition in $Cr_{1.04}Te_2$, we conducted measurements of isothermal magnetization near its T_C, and further analyzed the critical exponents correlated to this transition. As illustrated in Fig. 3(a), we measured the M–H curves at 2 K intervals with an in-plane field due to its easy axis between 224 K and 266 K. Typically, the mean-field model, utilizing Arrott plots of M^2 versus H/M, is used to estimate critical exponents preliminarily.[53] Within the hypothetical mean-field model, Arrott plots should ideally consist of parallel lines in the high-magnetic-field sections. However, the plots instead demonstrate a downward curvature and lack parallel alignment in these high-field areas [Fig. 3(b)], pointing out the inadequacy of the mean-field model for $Cr_{1.04}Te_2$. This discrepancy is attributed to the neglect of Coulomb correlation and spin fluctuation effects in this model, which play significant roles in ferromagnetic materials.[54] Moreover, the Banerjee criterion allows determination of the order of the phase transition by means of the slope of Arrott plots: a positive slope in the M^2 versus H/M curves signifies a second-order transition, whereas a negative slope suggests a first-order transition.[55] Obviously, the observed positive slope confirms that the transition from paramagnetic state (PM) to ferromagnetic state (FM) in $Cr_{1.04}Te_2$ is of the second order.

For second-order magnetic phase transitions, critical exponents, such as β, γ, and δ, can be determined by the following series of equations:[56,57]

$$M_S(T) = M_0(-\varepsilon)^{\beta}, \quad \varepsilon < 0, \quad T < T_C, \tag{1}$$

$$\chi_0^{-1}(T) = (H_0/M_0)(\varepsilon)^{\gamma}, \quad \varepsilon > 0, \quad T > T_C, \tag{2}$$

$$M = DH^{1/\delta}, \quad \varepsilon = 0, \quad T = T_C, \tag{3}$$

where $\varepsilon = (T - T_C)/T_C$ is the reduced temperature and M_0, H_0/M_0, and D are the critical amplitudes. For broader applications, the Arrott–Noaks equation of state modifies the Arrott plot by[58]

$$(H/M)^{1/\gamma} = (T - T_C)/T_C + (M/M_1)^{1/\beta}, \tag{4}$$

where M_1 is a constant. Given the inadequacy of the mean-field model for $Cr_{1.04}Te_2$, we explore various critical behaviors, such as (i) the 3D Heisenberg model ($\beta = 0.365$, $\gamma = 1.336$),[59] (ii) the 3D Ising model ($\beta = 0.325$, $\gamma = 1.24$),[59] (iii) the tricritical mean-field model ($\beta = 0.25$, $\gamma = 1.0$),[60] (iv) the 3D XY model ($\beta = 0.345$, $\gamma = 1.316$),[61] and (v) the 2D Ising model ($\beta = 0.125$, $\gamma = 1.75$).[61] Modified Arrott plots (MAP) of $M^{1/\beta}$ versus $(H/M)^{1/\gamma}$ curves based on these models are illustrated in Figs. 3(c)–3(g). Ideally, the high-field-region MAP should display parallel lines. However, determining the most suitable model is challenging, as all 3D models display nearly straight lines. By comparing the slope of the $M^{1/\beta}$ versus $(H/M)^{1/\gamma}$ curve to which T_C belongs, and calculating the normalized slope $[NS = S(T)/S(T_C)]$ for different temperatures, one may identify an appropriate model. NS would be a constant of 1 regardless of the temperature if the model is suitable. It is worth noting that this method only offers an empirical approach to facilitate the judgment of subsequent critical exponents, but it cannot determine the final model. Figure 3(h) shows the temperature-dependent NS for these models, highlighting the 2D Ising model has a significant deviation, while the NS of 3D Ising model is closest to 1.

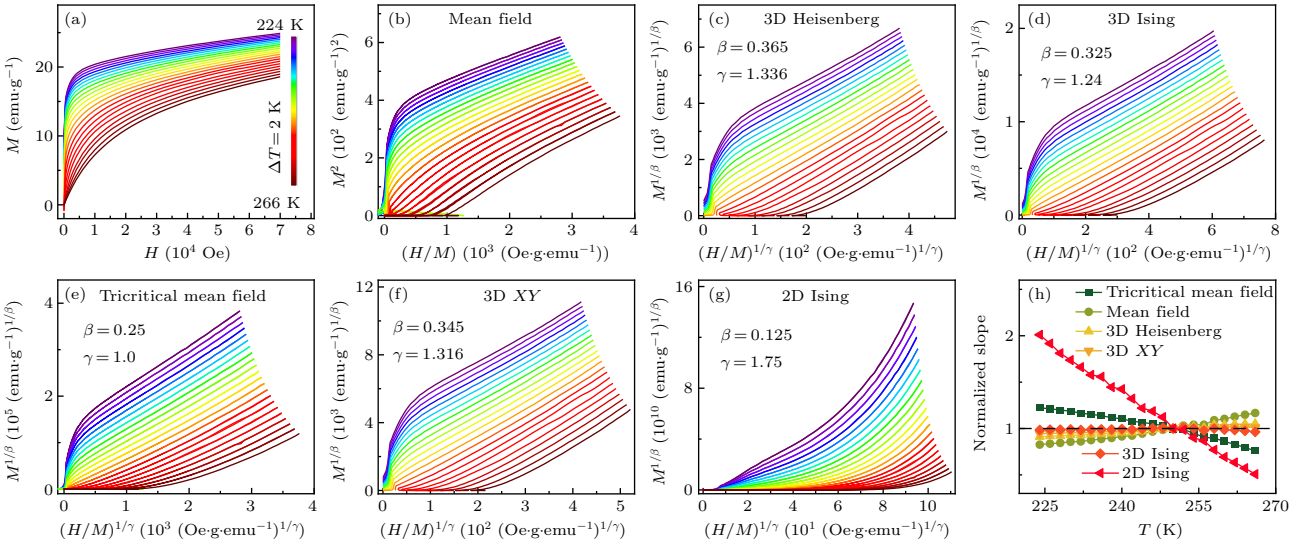


Fig. 3. (a) Isothermal magnetization (M–H) at different temperatures around T_C measured in-plane. The modified Arrott plots of $M^{1/\beta}$ versus $(H/M)^{1/\gamma}$ with parameters of (b) mean-field model, (c) 3D-Heisenberg model, (d) 3D-Ising model, (e) tricritical mean-field model, (f) 3D-XY model, and (g) 2D-Ising model. (h) Temperature dependence of the normalized slopes, $NS = S(T)/S(T_C)$, for different models. The black dashed line is a basic line of $NS = 1$.

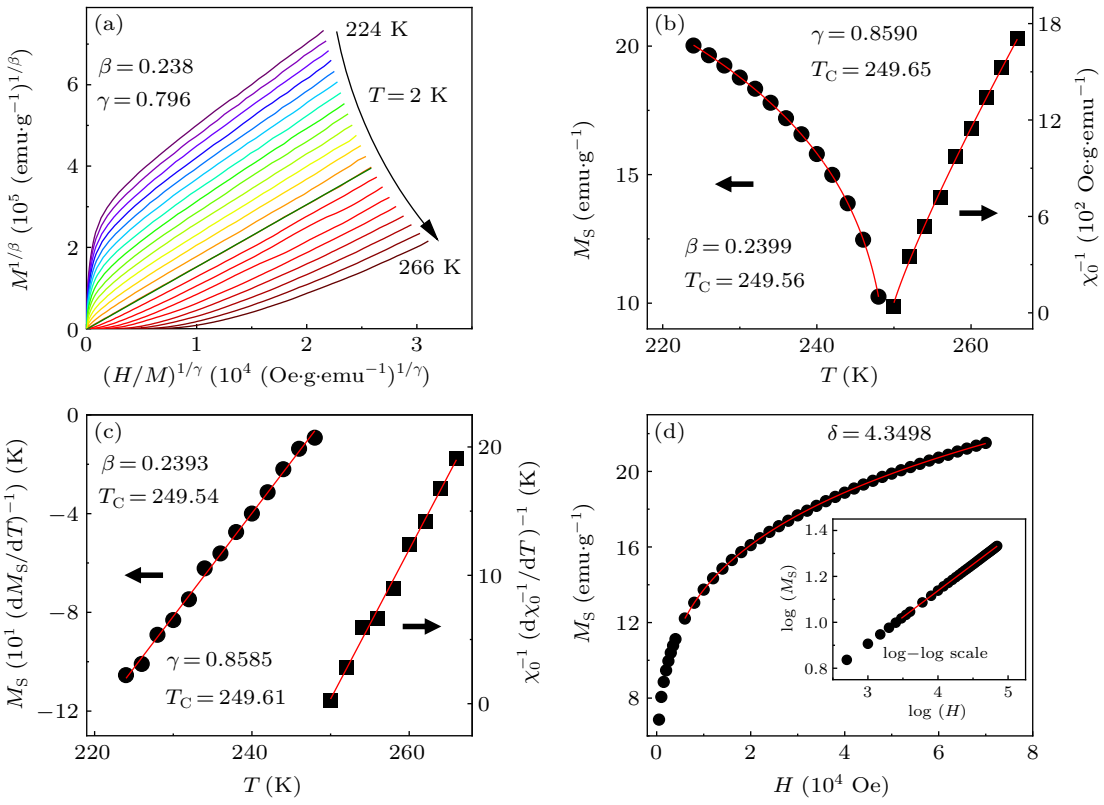


Fig. 4. (a) Modified Arrott plots of $M^{1/\beta}$ versus $(H/M)^{1/\gamma}$ with the parameters of $\beta = 0.238$ and $\gamma = 0.796$. (b) Temperature-dependent magnetization $M_S(T)$ for $T < 250$ K and $\chi_0^{-1}(T)$ for $T \geq 250$ K. The red solid lines are the fitting curves complying with Eqs. (1) and (2). (c) Kouvel–Fisher plots show the temperature dependence of $M_S/[\mathrm{d}M_S(T)/\mathrm{d}T]$ (circles) and $\chi_0^{-1}/[\mathrm{d}\chi_0^{-1}(T)/\mathrm{d}T]$ (squares) for $Cr_{1.04}Te_2$. The red solid lines are the fitting curves complying with Eqs. (4) and (5). (d) The isotherm M–H curve measured at $T_C = 250$ K and its fitting by Eq. (3). The inset shows the corresponding log–log scale representation.

To obtain the more accurate critical exponents, we utilize a thorough iterative technique. This involves linearly fitting the high-field correction curves to the $M^{1/\beta}$ and $(H/M)^{1/\gamma}$ axes in the MAP, then extrapolating to reliably determine M_S and χ_0^{-1}. Applying Eqs. (1) and (2) to these values allows us to calculate β and γ, leading to the creation of a new MAP. This step is repeated, deriving a new set of β and γ each time, until these values stabilize. The exponents thus obtained are not dependent on the initial estimates, ensuring their accuracy. As illustrated in Fig. 4(a), after several iterations, the MAP with

$\beta = 0.238$ and $\gamma = 0.796$ is established. The solid green line represents a linear fit of the isothermal magnetization curve at 250 K, nearly reaching the coordinate origin in Fig. 4(a), suggesting that T_C is approximately 250 K. Employing the Pramanik and Banerjee criteria,[62] we plot the temperature-dependent $M_S(T)$ for $T < 250$ K and $\chi_0^{-1}(T)$ for $T \geq 250$ K, achieving excellent fits as shown in Fig. 4(b). The final values are $\beta = 0.2399$ with $T_C = 249.56$ K, and $\gamma = 0.8590$ with $T_C = 249.65$ K. Details of the iteration process can be referred to the supplementary materials.

To confirm the critical exponents of $Cr_{1.04}Te_2$ derived through the MAP method, the Kouvel–Fisher method is utilized for verification as[63]

$$\frac{M_S(T)}{\mathrm{d}M_S(T)/\mathrm{d}T} = \frac{T - T_C}{\beta}, \tag{5}$$

$$\frac{\chi_0^{-1}(T)}{\mathrm{d}\chi_0^{-1}(T)/\mathrm{d}T} = \frac{T - T_C}{\gamma}. \tag{6}$$

This approach indicates that the temperature-dependent ratios of $M_S/(\mathrm{d}M_S/\mathrm{d}T)$ and $\chi_0^{-1}/(\mathrm{d}\chi_0^{-1}/\mathrm{d}T)$ plot as straight lines, with slopes corresponding to $1/\beta$ and $1/\gamma$, respectively. Linear fits below and above T_C yield $\beta = 0.2393$ with $T_C = 249.54$ K and $\gamma = 0.8585$ with $T_C = 249.61$ K, as depicted in Fig. 4(c). These β, γ, and T_C values, confirmed by the KF method, are similar to those obtained through the iterative MAP, further confirming the accuracy and reliability of the critical values.

To verify, the critical exponents are examined based on their interconnected characteristics. According to Eq. (3), the M–H at T_C is expected to follow a curve defined by a $1/\delta$ exponent, resulting in a straight line with a slope of $1/\delta$ on a log–log plot. Figure 4(d) displays the M–H isothermal magnetization at 250 K, with its log–log scale representation in the inset, yielding $\delta = 4.3498$. Moreover, the critical exponents β, γ, and δ adhere to the Widom scaling relation[64]

$$\delta = 1 + \frac{\gamma}{\beta}, \tag{7}$$

the corresponding $\delta = 4.579$ and $\delta = 4.472$ are calculated based on the critical exponents obtained via the MAP and KF methods, respectively. The δ values derived from critical isotherm analyses closely match those predicted by the Widom scaling law, underscoring the reliability and consistency of the critical exponents determined in our research, within the scope of experimental error.

Scaling analysis further confirms the accuracy of the determined critical exponents. With appropriate parameters, the magnetization and magnetic field conform to the following equation:[56]

$$M(H,\varepsilon) = \varepsilon^{\beta} f_{\pm}\left(\frac{H}{\varepsilon^{(\beta+\gamma)}}\right), \tag{8}$$

where $f_{\pm}$ represent specific functions for $T > T_C$ and $T < T_C$, respectively. By defining the renormalized magnetic field $h \equiv \varepsilon^{-(\beta+\gamma)}H$, and the magnetization strength $m \equiv \varepsilon^{-\beta}M(H,\varepsilon)$, Eq. (8) simplifies to

$$m = f_{\pm}(h). \tag{9}$$

This indicates that with accurately chosen β, γ, and δ, the plots of m versus h should consolidate into two distinct curves for $T > T_C$ and $T < T_C$ in the high-field regime. As illustrated in Fig. 5(a), the normalized magnetization intensity m against the normalized field h indeed merges into two separate curves for temperatures above and below T_C in the high-field region. The validity of the critical exponents and T_C has been solidified by a more rigorous method, illustrated by the m^2 against h/m graph in Fig. 5(b). Here, the data distinctly align along two separate branches for temperatures above and below T_C, which strongly suggests that the interactions are correctly normalized within the critical region, in accordance with the scaling law.

In addition, a variant of the scalar equation is given by[59]

$$\frac{H}{M^{\delta}} = k\left(\frac{\varepsilon}{H^{1/\beta}}\right), \tag{10}$$

where $k(x)$ is the scaling function. This equation implies that all experimental data, for temperatures both above and below T_C, should align along a single curve,[59] which has been demonstrated in the inset of Fig. 5(b). All high-field data conform to the universal curve $MH^{-1/\delta}$ versus $\varepsilon H^{-1/(\beta\delta)}$, pointing the curve at the zero point of the horizontal axis as corresponding to the T_C. This validates and substantiates the critical exponents derived from our experimental findings, affirming their accuracy and reliability.

Table 1 presents a comprehensive summary of critical indices derived from different methods alongside theoretical predictions from different models. The experimentally obtained critical exponents β, γ, and δ closely align with those predicted by the tricritical mean-field model.[65] This clearly demonstrates a tricritical phenomenon occurring at the boundary between first-order and second-order transitions, which has been evidenced in the m versus h curves in the low-field region [Fig. 5(c)]. Unlike the convergence into a single curve at high fields [Fig. 5(a)], the curves at low field diverge. The divergence observed in the low-field region may suggest a more complicated magnetic ordering.[48] Thus, a magnetic phase diagram illustrating this tricritical phenomenon is plotted in Fig. 5(d), pinpointing a tricritical point at 250 K and 480 Oe. At low fields below T_C, the phase may transition from multidomain to single domain[30] or involve a ferromagnetic and antiferromagnetic competition, as theorized and observed in Cr_xTe_2 compounds.[26,38,66] Additionally, we have compiled critical exponents and their models for other 2D vdW ferromagnetic materials in Table 2.

The compatibility of $Cr_{1.04}Te_2$ with the tricritical mean-field model suggests the presence of long-range magnetic interactions. The category of magnetic phase transitions in a uniform magnet is influenced by the exchange range, $J(r)$. Theoretical analysis by Fisher *et al*. describes magnetic ordering as an attraction between spins, with renormalization group theory indicating that the strength of interaction decreases as distance r increases, described by $J(r) \sim r^{-(d+\sigma)}$, with d denoting spatial dimensions and σ a positive constant.[57] Moreover, γ can be written as follows:[67]

$$\gamma = 1 + \frac{4}{d}\left(\frac{n+2}{n+8}\right)\Delta\sigma + \frac{8(n+2)(n-4)}{d^2(n+8)^2} \times \left[1 + \frac{2G(d/2)(7n+20)}{(n-4)(n+8)}\right]\Delta\sigma^2, \tag{11}$$

where $\Delta\sigma = (\sigma - d/2)$ and $G(d/2) = 3 - (1/4)(d/2)^2$. Specifically, the dimensionality of lattice and spin, denoted by n, influences the magnetic behavior. In 3D isotropic magnets where $\sigma > 2$, the 3D Heisenberg model applies, characterized by a magnetic exchange, $J(r)$, declining more rapidly than r^{-5}, indicative of short-range interactions. Conversely, mean-field exponents emerge when $J(r)$ falls off more slowly than $r^{-4.5}$. For σ values between 3/2 and 2, the system falls into a unique category with critical exponents varying with σ. In $Cr_{1.04}Te_2$, it is found that the distance of magnetic exchange, $J(r) \sim r^{-4.1}$ ($d = 3$), indicates slow decay of spin interaction with distance, classifying it within the realm of long-range interactions, which is in line with other systems described by the tricritical mean-field model.[65]

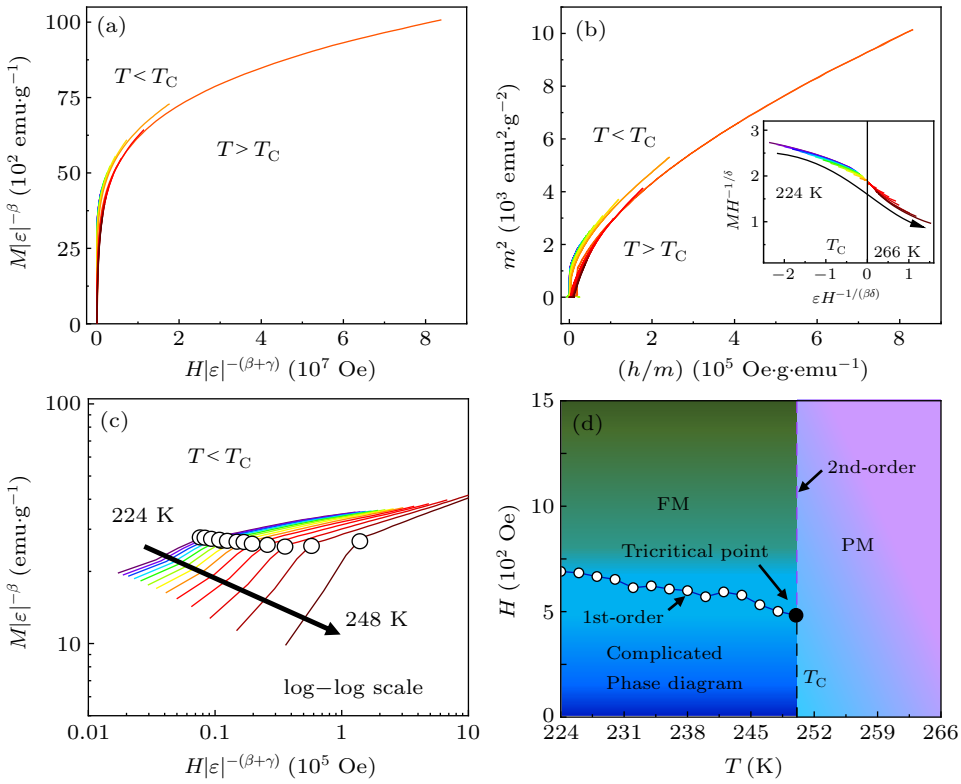


Fig. 5. (a) Scaling plots of the normalized magnetization intensity m versus normalized field h for $Cr_{1.04}Te_2$. (b) Renormalized magnetization intensity m^2 as a function of h/m. The inset is a rescaling of the M–H curve by $MH^{-1/\delta}$ versus $\varepsilon H^{-1/(\beta\delta)}$. (c) The log–log scale of the scaling plots below T_C at low magnetic field. (d) The magnetic phase diagram with tricritical phenomenon.

Table 1. Comparison of critical exponents of $Cr_{1.04}Te_2$ with different theoretical models.

Composition	Technique	T_C (K)	β	γ	δ	Reference
$Cr_{1.04}Te_2$	modified Arrott plot	249.56(4)	0.2399(14)	0.8590(582)	4.579	this work
	Kouvel–Fisher plot	249.61(29)	0.2393(36)	0.8585(254)	4.472	
	critical isotherm				4.3498(40)	
2D-Ising	theory		0.125	1.75	15	[61]
3D-Ising	theory		0.325	1.24	4.82	[59]
3D-*XY*	theory		0.345	1.316	4.81	[61]
3D-Heisenberg	theory		0.365	1.386	4.8	[59]
Mean-field	theory		0.5	1.0	3	[53]
Tricritical mean-field	theory		0.25	1.0	5	[60]

Table 2. Comparison of critical exponents of $Cr_{1.04}Te_2$ with other vdW magnets.

Composition	Technique	T_C (K)	β	γ	δ	model	Reference
$Cr_{1.04}Te_2$	MAP	249.56(4)	0.2399(14)	0.8590(582)	4.579	tricritical mean field	this work
	KF	249.61(29)	0.2393(36)	0.8585(254)	4.472		
	critical isotherm				4.3498(40)		
Cr_4Te_5	MAP	319.06(9)	0.388(4)	1.290(8)	4.32(3)	3D Heisenberg	[34]
	KF	318.90(9)	0.387(9)	1.288(5)	4.32(2)		
Cr_5Te_6	MAP	338.170(1)	0.405(1)	1.200(1)	3.962(2)	between the mean field and the 3D Heisenberg	[51]
	KF	338.13(0)	0.406(2)	1.199(5)	3.95(3)		
Cr_5Te_8	MAP	222.13(4)	0.327(4)	1.26(1)	4.9(1)	3D Ising	[50]
	KF	222.0(4)	0.321(7)	1.27(2)	4.9(2)		
$Cr_{0.62}Te$	MAP	230.76(9)	0.314(7)	1.83(2)	6.83(7)		[37]
	KF	230.65(26)	0.315(7)	1.81(2)	6.75(6)		
$CrSiTe_3$	MAP	31.06(9)	0.170(8)	1.532(1)	10.012(47)	2D Ising	[68]
	KF	31.09(2)	0.170(8)	1.532(1)	9.925(56)		
$CrGeTe_3$	MAP	67.95(5)	0.242(6)	0.985(3)	5.07(6)	Tricritical mean field	[69]
	KF	67.91(7)	0.240(6)	1.000(5)	5.167(6)		
Fe_5GeTe_2	MAP	237.76(3)	0.344(5)	1.406(1)	5.02(6)	3D Heisenberg	[70]
	KF	273.75(7)	0.346(4)	1.364(9)	4.94(0)		
Fe_4GeTe_2	MAP	270.22(7)	0.37(1)	1.21(3)	4.24(2)		[70]
	KF	270.2(2)	0.376(19)	1.20(5)	4.22(14)		
$FeTa_3S_6$	MAP	35.2	0.189(2)	1.423(1)	8.53(7)	2D Ising	[46]
Fe_3GaTe_2	MAP	358.06(13)	0.350(6)	1.388(34)	4.97(12)	3D Heisenberg	[45,48]
	KF	358.07(1)	0.350(1)	1.385(5)	4.96(2)		

3. Method

Single crystals of $Cr_{1.04}Te_2$ were bought from the PrMat company, which were grown by reacting potassium, Cr, and Te followed by a deintercalation step to remove the potassium. In addition, the stoichiometry was investigated using energy-dispersive x-ray spectroscopy in a Zeiss MER-LIN scanning electron microscope. Magnetic properties were measured by using a superconducting quantum interference device (SQUID) magnetometer (MPMS3, Quantum Design).

4. Conclusion

In summary, basic magnetic measurements have been carried out on the quasi-2D vdW ferromagnet $Cr_{1.04}Te_2$, and then its critical behavior is investigated in detail in this paper. The PM–FM phase transition in $Cr_{1.04}Te_2$ is found to be of second order. The critical exponents $\beta = 0.2399$, $\gamma = 0.8590$, and $\delta = 4.3498$ are successfully obtained by the MAP method with the KF method and their veracity is confirmed by the scaling equation. The $Cr_{1.04}Te_2$ demonstrates a stronger resemblance to the tricritical mean-field model with long-range interaction. Our research unveils a quasi-2D ferromagnetic metal that could be useful for the study of critical behavior and engineering vdW spintronic heterostructures.

Acknowledgments

Project supported by the Natural Science Foundation of Nanjing University of Posts and Telecommunications (Grant No. NY222170), Jiangsu Specially-Appointed Professor Program, and Natural Science Foundation of Universities of Jiangsu Province (Grant No. TJ219008). X.Z. acknowledges the support of the open research fund of Key Laboratory of Quantum Materials and Devices (Southeast University), Ministry of Education.

References

[1] Liu Y, Duan X, Shin H J, Park S, Huang Y and Duan X 2021 *Nature* **591** 43
[2] Lin X, Yang W, Wang K L and Zhao W 2019 *Nat. Electron.* **2** 274
[3] Gong C, Li L, Li Z, Ji H, Stern A, Xia Y, Cao T, Bao W, Wang C, Wang Y, Qiu Z Q, Cava R J, Louie S G, Xia J and Zhang X 2017 *Nature* **546** 265
[4] Huang B, Clark G, Navarro-Moratalla E, Klein D R, Cheng R, Seyler K L, Zhong D, Schmidgall E, McGuire M A, Cobden D H, Yao W, Xiao D, Jarillo-Herrero P and Xu X 2017 *Nature* **546** 270
[5] Zhu W, Zhu Y, Zhou T, Zhang X, Lin H, Cui Q, Yan F, Wang Z, Deng Y, Yang H, Zhao L, Žutić I, Belashchenko K D and Wang K 2023 *Nat. Commun.* **14** 5371
[6] Yin S, Zhao L, Song C, Huang Y, Gu Y, Chen R, Zhu W, Sun Y, Jiang W, Zhang X and Pan F 2021 *Chin. Phys. B* **30** 027505
[7] Deng Y, Yu Y, Song Y, Zhang J, Wang N Z, Sun Z, Yi Y, Wu Y Z, Wu S, Zhu J, Wang J, Chen X H and Zhang Y 2018 *Nature* **563** 94
[8] Zhang G, Guo F, Wu H, Wen X, Yang L, Jin W, Zhang W and Chang H 2022 *Nat. Commun.* **13** 5067
[9] Zhang H, Raftrey D, Chan Y T, Shao Y T, Chen R, Chen X, Huang X, Reichanadter J T, Dong K, Susarla S, Caretta L, Chen Z, Yao J, Fischer P, Neaton J B, Wu W, Muller D A, Birgeneau R J and Ramesh R 2022 *Sci. Adv.* **8** eabm7103

[10] Wu Z, Niu W, Li W, Yang J, Gu K, Liu X, Wang X, Chang S, Wei L, Li F, Liu P, Zhang X, Ma J, He L, Xu Y and Pu Y 2023 *Appl. Phys. Lett.* **123** 192403

[11] Huang K, Li Z, Guo D, Yang H, Li Y, Liang A, Wu F, Xu L, Yang L, Ji W, Guo Y, Chen Y and Liu Z 2022 *Chin. Phys. B* **31** 057404

[12] Li W, Zhu W, Zhang G, Wu H, Zhu S, Li R, Zhang E, Zhang X, Deng Y, Zhang J, Zhao L, Chang H and Wang K 2023 *Adv. Mater.* **35** 2303688

[13] Zhu W, Xie S, Lin H, Zhang G, Wu H, Hu T, Wang Z, Zhang X, Xu J, Wang Y, Zheng Y, Yan F, Zhang J, Zhao L, Patané A, Zhang J, Chang H and Wang K 2022 *Chin. Phys. Lett.* **39** 128501

[14] Zhang X, Lu Q, Liu W, Niu W, Sun J, Cook J, Vaninger M, Miceli P F, Singh D J, Lian S W, Chang T R, He X, Du J, He L, Zhang R, Bian G and Xu Y 2021 *Nat. Commun.* **12** 2492

[15] Chen Y, Zhu Y, Lin R, Niu W, Liu R, Zhuang W, Zhang X, Liang J, Sun W, Chen Z, Hu Y, Song F, Zhou J, Wu D, Ge B, Yang H, Zhang R and Wang X 2023 *Adv. Funct. Mater.* **33** 2302984

[16] Zhang X, Liu W, Niu W, Lu Q, Wang W, Sarikhani A, Wu X, Zhu C, Sun J, Vaninger M, Miceli P F, Li J, Singh D J, Hor Y S, Zhao Y, Liu C, He L, Zhang R, Bian G, Yu D and Xu Y 2022 *Adv. Funct. Mater.* **32** 2202977

[17] Zhou J, Song X, Chai J, Wong N L M, Xu X, Jiang Y, Feng Y P, Yang M and Wang S 2022 *J. Alloys Compd.* **893** 162223

[18] Fan X, Xin R, Li L, Zhang B, Li C, Zhou X, Chen H, Zhang H, OuYang F and Zhou Y 2023 *Front. Phys.* **19** 23401

[19] Lv H Y, Lu W J, Shao D F, Liu Y and Sun Y P 2015 *Phys. Rev. B* **92** 214419

[20] Yang J, Zhu C, Deng Y, Tang B and Liu Z 2023 *iScience* **26** 106567

[21] Huang M, Wang S, Wang Z, Liu P, Xiang J, Feng C, Wang X, Zhang Z, Wen Z, Xu H, Yu G, Lu Y, Zhao W, Yang S A, Hou D and Xiang B 2021 *ACS Nano* **15** 9759

[22] Freitas D C, Weht R, Sulpice A, Remenyi G, Strobel P, Gay F, Marcus J and Nunez-Regueiro M 2015 *J. Phys.: Condens Matter.* **27** 176002

[23] Zheng H, Huang C, Lin F, Fan J, Liu H, Zhang L, Ma C, Wang C, Zhu Y and Yang H 2023 *Appl. Phys. Lett.* **122** 023103

[24] Huang M, Ma Z, Wang S, Li S, Li M, Xiang J, Liu P, Hu G, Zhang Z, Sun Z, Lu Y, Sheng Z, Chen G, Chueh Y L, Yang S A and Xiang B 2021 *2D Mater.* **8** 031003

[25] Meng L, Zhou Z, Xu M, Yang S, Si K, Liu L, Wang X, Jiang H, Li B, Qin P, Zhang P, Wang J, Liu Z, Tang P, Ye Y, Zhou W, Bao L, Gao H J and Gong Y 2021 *Nat. Commun.* **12** 809

[26] Xian J J, Wang C, Nie J H, Li R, Han M, Lin J, Zhang W H, Liu Z Y, Zhang Z M, Miao M P, Yi Y, Wu S, Chen X, Han J, Xia Z, Ji W and Fu Y S 2022 *Nat. Commun.* **13** 257

[27] Ou Y, Yanez W, Xiao R, Stanley M, Ghosh S, Zheng B, Jiang W, Huang Y S, Pillsbury T, Richardella A, Liu C, Low T, Crespi V H, Mkhoyan K A and Samarth N 2022 *Nat. Commun.* **13** 2972

[28] Zhang X, Ambhire S C, Lu Q, Niu W, Cook J, Jiang J S, Hong D, Alahmed L, He L, Zhang R, Xu Y, Zhang S S L, Li P and Bian G 2021 *ACS Nano* **15** 15710

[29] Liu X, Huang P, Xia Y, Gao L, Liao L, Cui B, Backes D, van der Laan G, Hesjedal T, Ji Y, Chen P, Zhang Y, Wu F, Wang M, Zhang J, Yu G, Song C, Chen Y, Liu Z, Yang Y, Peng Y, Li G, Yao Q and Kou X 2023 *Adv. Funct. Mater.* **33** 2304454

[30] Zhang X, Li Y, Lu Q, Xiang X, Sun X, Tang C, Mahdi M, Conner C, Cook J, Xiong Y, Inman J, Jin W, Liu C, Cai P, Santos E J G, Phatak C, Zhang W, Gao N, Niu W, Bian G, Li P, Yu D and Long S 2024 *Adv. Mater.* 2311591

[31] Zhang C, Liu C, Zhang J, Yuan Y, Wen Y, Li Y, Zheng D, Zhang Q, Hou Z, Yin G, Liu K, Peng Y and Zhang X X 2023 *Adv. Mater.* **35** 2205967

[32] Wu H, Zhang W, Yang L, Wang J, Li J, Li L, Gao Y, Zhang L, Du J, Shu H and Chang H 2021 *Nat. Commun.* **12** 5688

[33] Liu J, Ding B, Liang J, Li X, Yao Y and Wang W 2022 *ACS Nano* **16** 13911

[34] Zhang L Z, Zhang A L, He X D, Ben X W, Xiao Q L, Lu W L, Chen F, Feng Z, Cao S, Zhang J and Ge J Y 2020 *Phys. Rev. B* **101** 214413

[35] Chua R, Zhou J, Yu X, Yu W, Gou J, Zhu R, Zhang L, Liu M, Breese M B H, Chen W, Loh K P, Feng Y P, Yang M, Huang Y L and Wee A T S 2021 *Adv. Mater.* **33** 2103360

[36] Wen Y, Liu Z, Zhang Y, Xia C, Zhai B, Zhang X, Zhai G, Shen C, He P, Cheng R, Yin L, Yao Y, Getaye Sendeku M, Wang Z, Ye X, Liu C, Jiang C, Shan C, Long Y and He J 2020 *Nano Lett.* **20** 3130

[37] Liu Y and Petrovic C 2017 *Phys. Rev. B* **96** 134410

[38] Tan C, Liao J H, Zheng G, Algarni M, Lin J Y, Ma X, Mayes E L H, Field M R, Albarakati S, Panahandeh-Fard M, Alzahrani S, Wang G, Yang Y, Culcer D, Partridge J, Tian M, Xiang B, Zhao Y J and Wang L 2023 *Phys. Rev. Lett.* **131** 166703

[39] Huang M, Gao L, Zhang Y, Lei X, Hu G, Xiang J, Zeng H, Fu X, Zhang Z, Chai G, Peng Y, Lu Y, Du H, Chen G, Zang J and Xiang B 2021 *Nano Lett.* **21** 4280

[40] Yan J, Luo X, Lin G, Chen F, Gao J, Sun Y, Hu L, Tong P, Song W, Sheng Z, Lu W, Zhu X and Sun Y 2019 *Europhys. Lett.* **124** 67005

[41] Yao J, Wang H, Yuan B, Hu Z, Wu C and Zhao A 2022 *Adv. Mater.* **34** 2200236

[42] Tang B, Wang X, Han M, Xu X, Zhang Z, Zhu C, Cao X, Yang Y, Fu Q, Yang J, Li X, Gao W, Zhou J, Lin J and Liu Z 2022 *Nat. Electron.* **5** 224

[43] Saha R, Meyerheim H L, Göbel B, Hazra B K, Deniz H, Mohseni K, Antonov V, Ernst A, Knyazev D, Bedoya-Pinto A, Mertig I and Parkin S S P 2022 *Nat. Commun.* **13** 3965

[44] Coughlin A L, Xie D, Zhan X, Yao Y, Deng L, Hewa-Walpitage H, Bontke T, Chu C W, Li Y, Wang J, Fertig H A and Zhang S 2021 *Nano Lett.* **21** 9517

[45] Algaidi H, Zhang C, Ma Y, Liu C, Chen A, Zheng D and Zhang X 2024 *APL Mater.* **12** 011124

[46] Rahman A, Rehman M U, Kiani M, Zhao H, Wang J, Lu Y, Ruan K, Dai R, Wang Z, Zhang L, Wang J and Zhang Z 2022 *Phys. Rev. B* **105** 144413

[47] Jiao Y Y, Sun J P and Cui Q 2021 *Chin. Phys. B* **30** 037501

[48] Chen Z, Yang Y, Ying T and Guo J G 2024 *Nano Lett.* **24** 993

[49] Wang X Y, Lin J F, Zeng X Y, Wang H, Ma X P, Wang Y T, Han K and Xia T L 2023 *Chin. Phys. Lett.* **40** 067503

[50] Zhang X, Yu T, Xue Q, Lei M and Jiao R 2018 *J. Alloys Compd.* **750** 798

[51] Zhang L Z, Xiao Q L, Chen F, Feng Z, Cao S, Zhang J and Ge J Y 2022 *J. Magn. Magn. Mater.* **546** 168770

[52] Liu H, Fan J, Zheng H, Wang J, Ma C, Wang H, Zhang L, Wang C, Zhu Y and Yang H 2023 *Front. Phys.* **18** 13302

[53] Arrott A 1957 *Phys. Rev.* **108** 1394

[54] Lamichhane T N, Xiang L, Lin Q, Pandey T, Parker D S, Kim T H, Zhou L, Kramer M J, Bud'ko S L and Canfield P C 2018 *Phys. Rev. Mater.* **2** 084408

[55] Banerjee S K 1964 *Phys. Lett.* **12** 16

[56] Stanley H E 1971 *Phase Transitions and Critical Phenomena*, Vol. 7 (Oxford: Clarendon Press)

[57] Fisher M E 1967 *Rep. Prog. Phys.* **60** 615

[58] Arrott A and Noakes J E 1967 *Phys. Rev. Lett.* **19** 786

[59] Kaul S 1985 *J. Magn. Magn. Mater.* **53** 5

[60] Kim D, Revaz B, Zink B, Hellman F, Rhyne J and Mitchell J 2002 *Phys. Rev. Lett.* **89** 227202

[61] Le Guillou J and Zinn-Justin J 1980 *Phys. Rev. B* **21** 3976

[62] Pramanik A K and Banerjee A 2009 *Phys. Rev. B* **79** 214426

[63] Kouvel J S and Fisher M E 1964 *Phys. Rev.* **136** A1626

[64] Widom B 1965 *J. Chem. Phys.* **43** 3898

[65] Zhang L, Menzel D, Jin C, Du H, Ge M, Zhang C, Pi L, Tian M and Zhang Y 2015 *Phys. Rev. B* **91** 024403

[66] Yang X, Zhou X, Feng W and Yao Y 2021 *Phys. Rev. B* **103** 024436

[67] Pramanik A K and Banerjee A 2009 *Phys. Rev. B* **79** 214426

[68] Liu B, Zou Y, Zhang L, Zhou S, Wang Z, Wang W, Qu Z and Zhang Y 2016 *Sci. Rep.* **6** 33873

[69] Lin G T, Zhuang H L, Luo X, Liu B J, Chen F C, Yan J, Sun Y, Zhou J, Lu W J, Tong P, Sheng Z G, Qu Z, Song W H, Zhu X B and Sun Y P 2017 *Phys. Rev. B* **95** 245212

[70] Li Z, Xia W, Su H, Yu Z, Fu Y, Chen L, Wang X, Yu N, Zou Z and Guo Y 2020 *Sci. Rep.* **10** 15345